
Benchmarking Self-Supervised Methods for Accelerated MRI Reconstruction

Andrew Wang¹ Mike Davies¹

Abstract

Reconstructing MRI from highly undersampled measurements is crucial for accelerating medical imaging, but is challenging due to the ill-posedness of the inverse problem. While supervised deep learning approaches have shown remarkable success, they rely on fully-sampled ground truth data, which is often impractical or impossible to obtain. Recently, numerous self-supervised methods have emerged that do not require ground truth, however, the lack of systematic comparison and standard experimental setups have hindered research. We present the first comprehensive review of loss functions from all feedforward self-supervised methods and the first benchmark on accelerated MRI reconstruction without ground truth, showing that there is a wide range in performance across methods. In addition, we propose **Multi-Operator Equivariant Imaging (MO-EI)**, a novel framework that builds on the imaging model considered in existing methods to outperform all state-of-the-art and approaches supervised performance. Finally, to facilitate reproducible benchmarking, we provide implementations of all methods in the [DeepInverse library](#) and easy-to-use [demo code here](#).

1. Introduction

Ill-posed inverse problems are ubiquitous in scientific and medical imaging and can be written as follows:

$$\mathbf{y}_i = \eta(A(\mathbf{x}_i)) \quad (1)$$

where $\mathbf{y}_i \in \mathbb{R}^m$ are measurements indexed by i , $\mathbf{x}_i \in \mathcal{X} \in \mathbb{R}^n$ are the underlying signals, $A(\cdot)$ is the forward operator and $\eta(\cdot)$ is the noise operator. The goal is to recover $\hat{\mathbf{x}} = f_\theta(\mathbf{y})$ via a solver f_θ , but $m < n$ in general, leading to an

ill-posed problem. In this work, we consider the problem of accelerated MRI reconstruction which is often modelled as a linear problem with Gaussian noise:

$$\mathbf{y}_{i,c} = \mathbf{A}_{i,c}\mathbf{x}_i + \epsilon, \quad \mathbf{A}_i = \mathbf{M}_i\mathbf{F}\mathbf{S}_c, \quad \epsilon \sim \mathcal{N}(0, \sigma) \quad (2)$$

where \mathbf{F} is a Fourier operator, $\mathbf{y}_{i,c}$ is the (i, c) -th measurement associated with the i -th undersampling mask \mathbf{M}_i and the c -th sensitivity map \mathbf{S}_c , and \mathbf{y} has dimension $\alpha = m = n/\alpha$ where α is the acceleration rate. We consider the scenario where measurements are single-coil $C = 1$ and noiseless $\sigma = 0$, thereby removing the effect of these somewhat orthogonal problems, in order to focus on tackling the ill-posedness of the problem, although the analysis easily generalises to the multi-coil scenario, and we discuss the noisy scenario in Section 2.2.1.

We emphasise that in MRI, the image set is often imaged through multiple operators $\mathbf{A}_i \sim \mathcal{A}$, via a random subsampling mask $\mathbf{M}_i \sim \mathcal{M}$. This assumption is often required for methods that learn from multiple operators, but we consider the single-operator case $\mathbf{A}_i = \mathbf{A} \forall i$ in Section 2.2.2.

The classical method of compressed sensing formulates the problem as regularised optimisation and is solved using variational inference (Aggarwal et al., 2019). However, these methods require hand-crafted priors, lengthy and expensive inference-time optimisation and acceleration rates may be limited.

Deep learning has been used to learn a solver directly from data, and achieved impressive results compared to classical methods. A popular framework which incorporates a learnt prior with classical data consistency is algorithm unrolling (Aggarwal et al., 2019), which performs finite iterations of the optimisation and replaces an element of the prior with a neural network, which is then trained end-to-end by alternating between denoising and data consistency steps to estimate $\hat{\mathbf{x}} = f_\theta(\mathbf{y}, \mathbf{A})$. Most methods assume that ground-truth (GT) data is available in order to train with supervised learning $\mathcal{L}_{\text{sup}} = \mathcal{L}(\hat{\mathbf{x}}, \mathbf{x}_{\text{GT}})$. These *feedforward* methods are desirable because they provide fast inference requiring only one forward pass as opposed to methods such as diffusion or other generative models which require lengthy iterations or optimisations at inference time.

¹Institute of Imaging, Data & Communications, School of Engineering, University of Edinburgh, UK. Correspondence to: Andrew Wang <andrew.wang@ed.ac.uk>.

However, fully-sampled GT measurements are often difficult or impossible to obtain in real scenarios, for example when imaging moving organs, or expensive, for lengthy high-resolution imaging. Self-supervised (a.k.a. unsupervised) learning is therefore needed to circumvent the need for GT, and numerous methods have been proposed in recent years. However they often fail to compare to existing methods, and it is difficult to draw direct comparisons due to variety in datasets, models, forward physics, or lack of clear implementation, hindering fast research and leading to poor applicability of these methods in practice. Recent surveys such as (Ongie et al., 2020; Zeng et al., 2021) mention various self-supervised methods included here, but lack a principled comparison, do not provide experimental results and mostly compare older methods.

We provide the first systematic survey of state-of-the-art self-supervised feedforward methods, and the first set of experimental results benchmarking these methods on accelerated MRI reconstruction without GT. Additionally, inspired by the benefits of these methods, we propose a new method which combines these into one framework. Finally, to facilitate reproducible benchmarking, we implement all compared methods using the DeepInverse library (Tachella et al., 2023), and provide a [demo notebook here](#).

1.1. Contributions

1. A benchmark comparison of state-of-the-art self-supervised feedforward methods for learning to reconstruct accelerated MRI without ground truth;
2. A new method, multi-operator equivariant imaging (MO-EI), that significantly outperforms all the above.

2. Related work

2.1. Benchmarked methods

We provide a systematic review of existing state-of-the-art feedforward self-supervised methods from the literature i.e. methods which only require measurements \mathbf{y} from a single acquisition at training and inference, without any ground truth. We formulate their loss functions and summarise all compared methods in Table 1 along with their implementations in the DeepInverse (Tachella et al., 2023) library. We focus on the design of the loss function since, in general, these loss functions are agnostic to the NN architecture and thus can be independently used with any latest architecture.

2.1.1. MEASUREMENT CONSISTENCY

The most naive self-supervised loss simply compares the recorrputed estimate $\mathbf{A}\hat{\mathbf{x}}$ to the measurement \mathbf{y} :

$$\mathcal{L}_{\text{MC}} = \mathcal{L}(\mathbf{A}\hat{\mathbf{x}}, \mathbf{y}) \quad (3)$$

where \mathcal{L} is any metric such as the L2 norm. This loss originally appeared with a classical regularising term to solve inverse problems with deep learning and traditional regularisation, but these still faced problems in designing the regularisers. Without a regularising term, the loss cannot recover information from the null-space of the operator $\mathcal{N}(\mathbf{A})$ as infinite solutions $\mathbf{A}^\top \mathbf{y} + \mathbf{v}$ can satisfy measurement consistency (MC) where $\mathbf{v} \in \mathcal{N}(\mathbf{A})$. This loss function is also used in the presence of strong inductive bias where the regularisation is provided by the architecture, for example from specific architectures (Darestani & Heckel, 2021) or initialisations (Darestani et al., 2022), or in cycle consistency losses (Oh et al., 2020).

2.1.2. LEARNING FROM MULTIPLE OPERATORS

A popular set of state-of-the-art approaches leverages the fact that the whole measurement space is spanned by multiple imaging operators. Measurement splitting methods, including SSDU (Yaman et al., 2020; Acar et al., 2021), randomly split the k-space into two sets at each iteration. One is used as the input and the other to construct the loss at the output:

$$\mathcal{L}_{\text{SSDU}} = \mathcal{L}(\mathbf{M}_2 \mathbf{A}_i f_\theta(\mathbf{M}_1 \mathbf{y}_i, \mathbf{M}_1 \mathbf{A}_i), \mathbf{M}_2 \mathbf{y}_i) \quad (4)$$

where \mathbf{M}_1 is a randomly generated mask, $\mathbf{M}_1 + \mathbf{M}_2 = \mathbb{I}_m$, and the inference-time estimate is $\hat{\mathbf{x}}_i = f_\theta(\mathbf{y}_i, \mathbf{A}_i)$. Note that some methods (Hu et al., 2024; Gan et al., 2021) require pairs of measurements of the same subject; these are equivalent to SSDU but with 2x less acceleration. Similarly, Artifact2Artifact (Gan et al., 2022; Liu et al., 2020), when applied to static MRI reconstruction without paired measurements, is also identical to SSDU (see Appendix A for proof). We therefore consider SSDU as the archetypal method to compare.

An inference-time adaptation to SSDU performs a Monte-Carlo averaging over subsampled inputs; this is inspired by Noise2Inverse (Hendriksen et al., 2020):

$$\hat{\mathbf{x}} = \frac{1}{N} \sum_{i=1}^N f_\theta(\mathbf{M}_i \mathbf{y}, \mathbf{M}_i \mathbf{A}) \quad (5)$$

More recently, (Millard & Chiew, 2023) frames SSDU as a Bernoulli-noise special case of Noisier2Noise (Moran et al., 2019), and propose a modification to the SSDU loss that improves its results.

Finally, Multi-Operator Imaging (MOI) (Tachella et al., 2022) leverages the fact that the image set is seen through multiple operators \mathbf{A}_i by drawing a random operator $\tilde{\mathbf{A}} \sim \mathcal{A}$ at each forward pass to learn in the null-space:

$$\mathcal{L}_{\text{MOI}} = \mathcal{L}_{\text{MC}} + \mathcal{L}(\hat{\mathbf{x}}, f_\theta(\tilde{\mathbf{A}}\hat{\mathbf{x}})) \quad (6)$$

Table 1.

Method	Ref	Loss	Implementation
MC	-	Eq. (3)	<code>dinv.loss.MCLoss()</code>
SSDU	(Yaman et al., 2020)	Eq. (4)	<code>dinv.loss.SplittingLoss(eval_split_input=False)</code>
Noise2Inverse	(Hendriksen et al., 2020)	Eq. (5)	<code>dinv.loss.SplittingLoss(eval_split_input=True)</code>
MOI	(Tachella et al., 2022)	Eq. (6)	<code>dinv.loss.MOILoss()</code>
EI	(Chen et al., 2021)	Eq. (7)	<code>dinv.loss.EILoss()</code>
MO-EI	Ours	Eq. (10)	<code>dinv.loss.MOEILoss()</code>

2.1.3. EQUIVARIANT IMAGING

Equivariant Imaging (EI) (Chen et al., 2021) is a state-of-the-art method that constrains the set of solutions using group invariance, which has been applied to MRI in (Chen et al., 2022), optical camera imaging in (Wang & Davies, 2024b), and dynamic MRI in (Wang & Davies, 2024a). By leveraging a natural assumption that the (unknown) image set \mathcal{X} is invariant to a group G of transformations $g\mathbf{x} \in \mathcal{X} \forall \mathbf{x} \in \mathcal{X}, g \in G$, the image set is observed through multiple transformed operators $\mathbf{A}_i \circ g(\cdot)$ allowing the solver to "see" into the null-space. The assumption is constrained using the following loss:

$$\mathcal{L}_{EI} = \mathcal{L}_{MC} + \mathcal{L}(\mathbf{T}_g \hat{\mathbf{x}}, f_\theta(\mathbf{A} \mathbf{T}_g \hat{\mathbf{x}})) \quad (7)$$

where $\mathbf{T}_g : G \rightarrow \text{Sym}(\mathcal{X})$ is an action of the group G .

2.1.4. DATA AUGMENTATION

EI is related to data augmentation (DA), which, when ground truth \mathbf{x}_{GT} is available, can be used to constrain invariance or equivariance on \mathbf{x} . While (Fabian et al., 2021) applies this to MRI, VORTEX (Desai et al., 2022a) performs data augmentation on inputs \mathbf{y} to attempt to solve the inverse problem.

2.1.5. ADVERSARIAL LOSSES

Adversarial losses have been proposed to reconstruct MRI via the dual training of a generator f_θ and a discriminator D . While unconditional, generative adversarial networks such as AmbientGAN (Bora et al., 2018) are not feedforward at inference time, (Cole et al., 2021) propose a feedforward method with an adversarial loss for training:

$$\mathcal{L}_{GAN} = D(\tilde{\mathbf{A}} f_\theta(\mathbf{y}), \tilde{\mathbf{y}}) \quad (8)$$

where $\tilde{\mathbf{y}} \sim \mathcal{Y}$ i.e. another randomly sampled measurement from the training dataset \mathcal{Y} . UAIR (Pajot et al., 2018) is a related method using the following loss:

$$\hat{\mathbf{y}} = \tilde{\mathbf{A}} f_\theta(\mathbf{y}), \mathcal{L}_{UAIR} = D(\hat{\mathbf{y}}, \mathbf{y}) + \mathcal{L}(\tilde{\mathbf{A}} f_\theta(\hat{\mathbf{y}}), \hat{\mathbf{y}}) \quad (9)$$

2.1.6. NON-FEEDFORWARD METHODS

Finally, we do not consider ground-truth-free methods that require inference or optimisation at inference-time, since these are impractical in real-world application, including Deep Image Prior methods (Darestani & Heckel, 2021), AmbientGAN (Bora et al., 2018), diffusion methods (Daras et al., 2023; Kawar et al., 2024), or implicit neural representation methods (Shen et al., 2024).

2.2. Other inverse problems

2.2.1. NOISY PROBLEMS

In this paper, we separate the task of solving ill-posed problems with removing measurement noise. To achieve the latter, it is often possible to add a denoising term to the loss function. For example, Robust EI (Chen et al., 2022) adds the Stein’s Unbiased Risk Estimator (SURE) term. Noise2Recon (Desai et al., 2022b) and Robust SSDU (Millard & Chiew, 2024) both add a term similar to Noisier2Noise (Moran et al., 2019) to perform denoising on top of SSDU.

For a comparison of state-of-the-art denoising methods in solving inverse problems, see (Tachella et al., 2025).

2.2.2. SINGLE-OPERATOR PROBLEMS

Many of the methods considered in Section 2.1 rely on the assumption that the image set is imaged with multiple operators, and that these operators span the full measurement domain in expectation. However, it is often the case, both in MRI and in general inverse problems, that all measurements are made with a single operator \mathbf{A} , for example a constant mask or blur kernel. In this case, we note that only the Equivariant Imaging (EI) losses (Chen et al., 2021) do not require the assumption and thus can still be used.

3. Our method

Motivated by the fact that adding more, well-targeted regularisation will typically improve the stability and generalisation of the model, we build upon the EI (Chen et al., 2021) and MOI (Tachella et al., 2022) losses to propose a hybrid Multi-Operator Equivariant Imaging (MO-EI) loss

function. Let \mathcal{A} be the operator set of order $|\mathcal{A}| = \binom{n}{m}$, as it is isomorphic to the mask index set of $m = n/\alpha$ -combinations of the index set \mathbb{I}_n . Define the *augmented operator set* $\mathcal{A}_G = \{\mathbf{A}_i \mathbf{T}_g \forall \mathbf{A}_i \in \mathcal{A}, g \in G\}$ as the orbit space of the set \mathcal{A} under the action of the group G , and assume that that these operators image the image set. Since $|\mathcal{A}_G| = |\mathcal{A}| |G|$ is much larger than in MOI or EI, we expect to be able to learn more information in the null-spaces of the operators and thereby improve the performance. We leverage the augmented operator set using the loss function:

$$\mathcal{L}_{\text{MO-EI}} = \mathcal{L}_{\text{MC}} + \mathcal{L}(\mathbf{T}_g \hat{\mathbf{x}}, f_\theta(\tilde{\mathbf{A}}_g \hat{\mathbf{x}})), \tilde{\mathbf{A}}_g \sim \mathcal{A}_G \quad (10)$$

The loss function is visualised diagrammatically in Fig. 1.

Remark (MO-EI generalises MOI and EI). *By letting G be the trivial group, we recover MOI (Tachella et al., 2022), and by letting $\mathcal{A} = \{\mathbf{A}\}$, we recover EI (Chen et al., 2021).*

For the group G , since we have soft deformable tissue (Gan et al., 2022), we expect \mathcal{X} be invariant to the group of C^1 -diffeomorphisms. As these are very general, we relax the full assumption and instead enforce approximate equivariance to small distortions (see Fig. 2) by taking the subset of continuous piecewise-affine-based diffeomorphic transforms from (Freifeld et al., 2017).

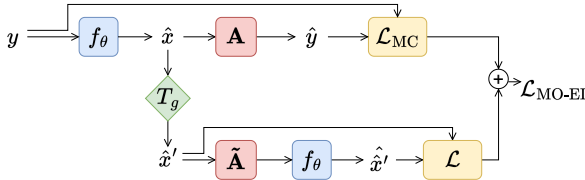


Figure 1. Our multi-operator equivariant imaging (MO-EI) framework.

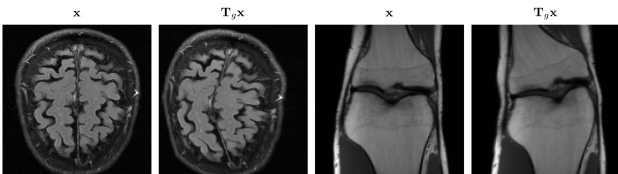


Figure 2. Diffeomorphic transforms.

4. Experiments

We compare all methods listed in Table 1, including state-of-the-art methods and our proposed method, using their implementations in the DeepInverse library (Tachella et al., 2023). We train a neural network network using a given

Loss	PSNR \uparrow	SSIM \uparrow
Zero-filled	27.67	.7862
MC	27.66	.7861
EI	30.26	.8523
MOI	30.29	.8651
SSDU	18.27	.4876
Noise2Inverse	18.49	.4693
MO-EI (ours)	32.14	.8846
(Supervised)	(33.15)	(.9032)

Table 2. Test set results for 6x accelerated MRI on FastMRI brain dataset. Best unsupervised method in **bold**.

loss on simulated measurements at 6x acceleration on brain and knee MRI data from the FastMRI dataset (Zbontar et al., 2018). We use a simple unrolled MoDL neural network from (Aggarwal et al., 2019) with a residual U-Net (Ronneberger et al., 2015) backbone and 3 unrolled iterations, and the same hyperparameters for all loss functions to provide fair comparisons. In addition, we train a model with supervised learning with access to oracle ground truth data, as a gold-standard comparison. We report PSNR and SSIM defined on the magnitude of the complex data. Further details on implementations of the various benchmarked loss functions, the dataset and experiment setup are in Appendix B.

We provide example code for how to train the reconstruction algorithm with the benchmarked methods in Appendix C, and provide full demo code here [at this URL](#).

Finally, we run further experiments to reproduce SSDU (Yaman et al., 2020) in Section 6.1 and test the robustness capabilities of our trained models to out-of-domain data in Section 6.2.

5. Results

Numerical results and sample reconstructions are shown for the brain dataset in Table 2 and Fig. 3 and for the knee dataset in Table 6 and Fig. 6. Note that all images are normalised to the range $[0, 1]$ before plotting. The no-learning zero-filled reconstruction is provided for reference. We provide an ablation of the components of our loss function (compared to MOI and EI) in Appendix D.

As expected, measurement consistency (MC) cannot learn any information and recovers the no-learning performance. While EI and MOI both show good results compared to MC, our method, MO-EI, improves significantly on both these previous state-of-the-art methods, approaches the oracle supervised learning performance, and recovers details in the brain images where EI and MOI have strong artifacts (see insets). While SSDU qualitatively seems to remove some artifacts compared to no-learning, its metrics

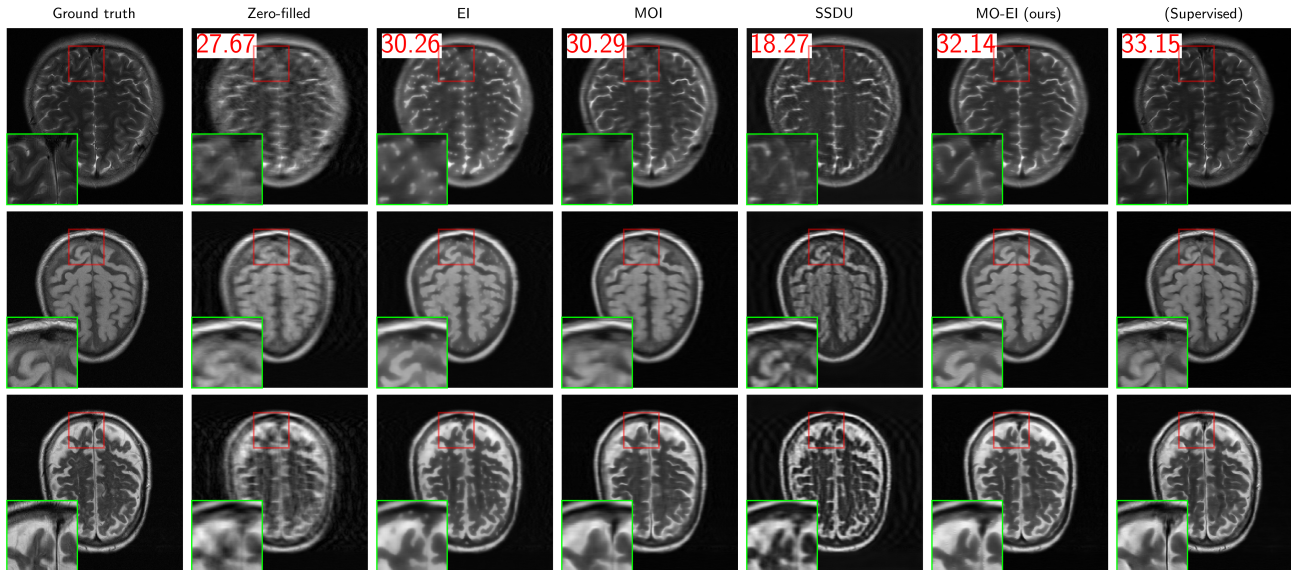


Figure 3. Sample reconstructions for 6x accelerated brain MRI reconstruction with average test-set PSNR labelled.

are very poor and drastically worse than no-learning; we explore why this is the case in Section 6.1.

6. Further experiments

6.1. Reproducing SSDU

We explore the seemingly poor performance of SSDU and attempt to reproduce the performance reported in (Yaman et al., 2020). First, we add 4 more unrolled iterations to the neural network from 3 to 7, increasing the training time by more-than-double. Note that this means these results are no longer directly comparable with other methods reported in Section 5. We observe a considerable qualitative performance increase but not quantitatively in Fig. 4 and Table 3. Then, noting that SSDU is trained on further subsampled measurements $M_1 y_i$ but tested on just the subsampled measurements y_i , we normalise the model output to the range $[0, 1]$. This improves the results, but removes any quantitative information in the pixel values. Finally, we standardise the output to the mean and standard deviation of the ground truth x . While this now shows an improvement over no-learning, this requires ground-truth statistics and thus would no longer be fully self-supervised. We note that the Noise2Inverse inference time procedure also does not help, differing from comparisons observed in dynamic MRI (Wang & Davies, 2024a).

6.2. Out-of-domain generalisation

Now suppose that ground truth data is available. We evaluate the robustness and generalisation of our models

Loss	PSNR \uparrow	SSIM \uparrow
Zero-filled	27.67	.7862
SSDU (3)	18.27	.4876
SSDU (7)	17.56	.4970
SSDU (7) normalised	26.75	.7525
SSDU (7) standardised	29.60	.8342
N2I (7) standardised	28.27	.7825

Table 3. Further results for training SSDU (Yaman et al., 2020) with a larger model (7 unrolled iters), and metrics after normalising output to $[0, 1]$ or standardising output (requires ground truth statistics \bar{x}_{GT}, σ_x).

Loss	PSNR \uparrow	SSIM \uparrow
Supervised	30.63	.7759
Self-sup	29.54	.7390
Interleaved	31.55	.7910

Table 4. Out-of-domain generalisation results for 6x accelerated MRI trained on the FastMRI brain dataset and tested on knees.

trained on brain data to out-of-domain, knee data. We compare a model trained with supervised learning on the brain data, our proposed self-supervised MO-EI method, and a model trained alternating between supervised and self-supervised (“interleaved”) losses. The results in Table 4 show that, even when ground truth is available, adding a self-supervised loss during supervised training significantly improves the robustness of the model. Qualitatively, the pure supervised model places strange brain artifacts in the knees in Fig. 5, where the interleaved training removes this while retaining a sharp image.

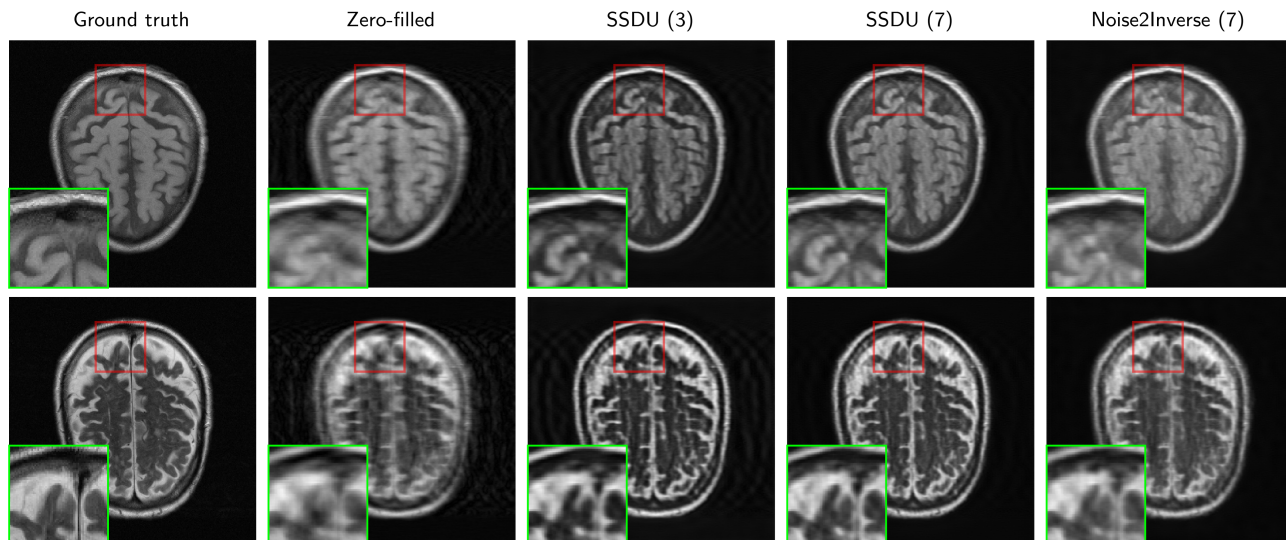


Figure 4. Sample reconstructions for further experiments on SSDU (Yaman et al., 2020) on brain data, where (3) represents a model with 3 unrolled iterations.

7. Conclusion

In this paper we provide an analysis of state-of-the-art self-supervised feedforward methods to train neural networks to solve the accelerated MRI reconstruction problem without ground-truth. We implement and benchmark these methods on fair experiments using real MRI data. We show that while some methods including EI and MOI (Chen et al., 2021; Tachella et al., 2022) show decent results, visible artifacts are still present in their reconstructions. We demonstrate that they generally outperform measurement-splitting methods including SSDU (Yaman et al., 2020), which we find requires a more expensive model and output standardisation to compete with measurement consistency, which cannot learn any more information than the zero-filled no-learning reconstruction. Furthermore, we propose a new method, multi-operator equivariant imaging (MOEI), which significantly outperforms all existing methods and approaches the performance of supervised learning. Additionally, in experiments where ground-truth is available, we show that adding the self-supervised loss during training considerably improves robustness to out-of-domain data. Finally, we provide easy-to-use implementations of all the benchmarked loss functions using the DeepInverse library (Tachella et al., 2023) which allows fast experimentation using cutting edge methods and custom datasets.

References

Acar, M., Çukur, T., and Öksüz, I. Self-supervised Dynamic MRI Reconstruction. In *Machine Learn-*

ing for Medical Image Reconstruction, pp. 35–44. Springer International Publishing, 2021. doi: 10.1007/978-3-030-88552-6_4.

Aggarwal, H. K., Mani, M. P., and Jacob, M. MoDL: Model-Based Deep Learning Architecture for Inverse Problems. *IEEE Transactions on Medical Imaging*, 38(2):394–405, February 2019. ISSN 1558-254X. doi: 10.1109/TMI.2018.2865356. URL <https://ieeexplore.ieee.org/document/8434321>. Conference Name: IEEE Transactions on Medical Imaging.

Bora, A., Price, E., and Dimakis, A. G. AmbientGAN: Generative models from lossy measurements. In *International Conference on Learning Representations*, February 2018.

Chen, D., Tachella, J., and Davies, M. E. Equivariant Imaging: Learning Beyond the Range Space. In *2021 IEEE/CVF International Conference on Computer Vision (ICCV)*, October 2021. doi: 10.1109/ICCV48922.2021.00434.

Chen, D., Tachella, J., and Davies, M. E. Robust Equivariant Imaging: a fully unsupervised framework for learning to image from noisy and partial measurements. In *2022 IEEE/CVF Conference on Computer Vision and Pattern Recognition (CVPR)*, June 2022. doi: 10.1109/CVPR52688.2022.00556.

Cole, E. K., Ong, F., Vasawala, S. S., and Pauly, J. M. Fast Unsupervised MRI Reconstruction Without Fully-Sampled Ground Truth Data Using Generative Adver-

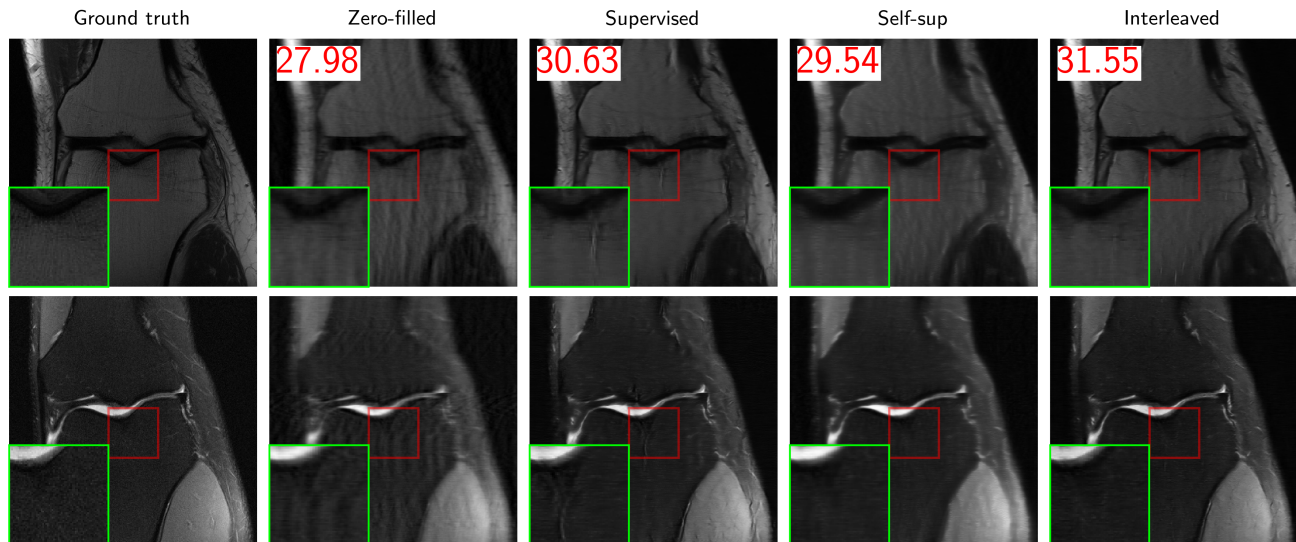


Figure 5. Sample reconstructions for out-of-domain generalisation experiments trained on 6x acc. brains and tested on 6x acc. knees with average test-set PSNR labelled.

- serial Networks. In *2021 IEEE/CVF International Conference on Computer Vision Workshops (ICCVW)*, pp. 3971–3980, October 2021. doi: 10.1109/ICCVW54120.2021.00444. URL <https://ieeexplore.ieee.org/document/9607486>. ISSN: 2473-9944.
- Daras, G., Shah, K., Dagan, Y., Gollakota, A., Dimakis, A. G., and Klivans, A. Ambient Diffusion: Learning Clean Distributions from Corrupted Data, May 2023. arXiv:2305.19256 [cs, math].
- Darestani, M. Z. and Heckel, R. Accelerated MRI with Untrained Neural Networks, April 2021. URL <http://arxiv.org/abs/2007.02471>. arXiv:2007.02471 [eess].
- Darestani, M. Z., Liu, J., and Heckel, R. Test-Time Training Can Close the Natural Distribution Shift Performance Gap in Deep Learning Based Compressed Sensing. In *Proceedings of the 39th International Conference on Machine Learning*, pp. 4754–4776. PMLR, June 2022. URL <https://proceedings.mlr.press/v162/darestani22a.html>. ISSN: 2640-3498.
- Desai, A. D., Gunel, B., Ozturkler, B. M., Beg, H., Vasawala, S., Hargreaves, B. A., Ré, C., Pauly, J. M., and Chaudhari, A. S. VORTEX: Physics-Driven Data Augmentations Using Consistency Training for Robust Accelerated MRI Reconstruction, June 2022a. URL <http://arxiv.org/abs/2111.02549>. arXiv:2111.02549 [eess].
- Desai, A. D., Ozturkler, B. M., Sandino, C. M., Boutin, R., Willis, M., Vasawala, S., Hargreaves, B. A., Ré, C. M., Pauly, J. M., and Chaudhari, A. S. Noise2Recon: Enabling Joint MRI Reconstruction and Denoising with Semi-Supervised and Self-Supervised Learning, October 2022b. URL <http://arxiv.org/abs/2110.00075>. arXiv:2110.00075 [eess].
- Fabian, Z., Heckel, R., and Soltanolkotabi, M. Data augmentation for deep learning based accelerated MRI reconstruction with limited data. In *Proceedings of the 38th International Conference on Machine Learning*, pp. 3057–3067, July 2021.
- Freifeld, O., Hauberg, S., Batmanghelich, K., and Fisher, J. W. Transformations Based on Continuous Piecewise-Affine Velocity Fields. *IEEE Transactions on Pattern Analysis and Machine Intelligence*, 39(12):2496–2509, December 2017. doi: 10.1109/TPAMI.2016.2646685. URL <https://ieeexplore.ieee.org/abstract/document/7814343>.
- Gan, W., Sun, Y., Eldeniz, C., Liu, J., An, H., and Kamilov, U. S. Deep Image Reconstruction Using Unregistered Measurements Without Groundtruth. In *2021 IEEE 18th International Symposium on Biomedical Imaging (ISBI)*, pp. 1531–1534, April 2021. doi: 10.1109/ISBI48211.2021.9434079. URL <https://ieeexplore.ieee.org/document/9434079>.
- Gan, W., Sun, Y., Eldeniz, C., Liu, J., An, H., and Kamilov, U. S. Deformation-Compensated Learning for Image

- Reconstruction Without Ground Truth. *IEEE Transactions on Medical Imaging*, 41(9):2371–2384, September 2022. ISSN 1558-254X. doi: 10.1109/TMI.2022.3163018.
- Hendriksen, A. A., Pelt, D. M., and Batenburg, K. J. Noise2Inverse: Self-Supervised Deep Convolutional Denoising for Tomography. *IEEE Transactions on Computational Imaging*, 6:1320–1335, 2020. doi: 10.1109/TCI.2020.3019647.
- Hu, Y., Gan, W., Ying, C., Wang, T., Eldeniz, C., Liu, J., Chen, Y., An, H., and Kamilov, U. S. SPICER: Self-Supervised Learning for MRI with Automatic Coil Sensitivity Estimation and Reconstruction, June 2024. URL <http://arxiv.org/abs/2210.02584>. arXiv:2210.02584 [eess].
- Kawar, B., Elata, N., Michaeli, T., and Elad, M. GSURE-Based Diffusion Model Training with Corrupted Data, June 2024. URL <http://arxiv.org/abs/2305.13128>. arXiv:2305.13128 [eess].
- Liu, J., Sun, Y., Eldeniz, C., Gan, W., An, H., and Kamilov, U. S. RARE: Image Reconstruction Using Deep Priors Learned Without Groundtruth. *IEEE Journal of Selected Topics in Signal Processing*, 14(6):1088–1099, October 2020. doi: 10.1109/JSTSP.2020.2998402. URL <https://ieeexplore.ieee.org/document/9103213>.
- Millard, C. and Chiew, M. A Theoretical Framework for Self-Supervised MR Image Reconstruction Using Sub-Sampling via Variable Density Noisier2Noise. *IEEE Transactions on Computational Imaging*, 9:707–720, 2023. doi: 10.1109/TCI.2023.3299212. URL <https://ieeexplore.ieee.org/document/10194985?denied=>.
- Millard, C. and Chiew, M. Clean self-supervised MRI reconstruction from noisy, sub-sampled training data with Robust SSDU, June 2024. URL <http://arxiv.org/abs/2210.01696>. arXiv:2210.01696 [eess].
- Moran, N., Schmidt, D., Zhong, Y., and Coady, P. Noisier2Noise: Learning to Denoise from Unpaired Noisy Data, October 2019. arXiv:1910.11908 [cs, eess].
- Oh, G., Sim, B., Chung, H., Sunwoo, L., and Ye, J. C. Unpaired Deep Learning for Accelerated MRI Using Optimal Transport Driven CycleGAN. *IEEE Transactions on Computational Imaging*, 6:1285–1296, 2020. ISSN 2333-9403. doi: 10.1109/TCI.2020.3018562. URL <https://ieeexplore.ieee.org/document/9173689>. Conference Name: IEEE Transactions on Computational Imaging.
- Ongie, G., Jalal, A., Metzler, C. A., Baraniuk, R. G., Dimakis, A. G., and Willett, R. Deep Learning Techniques for Inverse Problems in Imaging. *IEEE Journal on Selected Areas in Information Theory*, 1(1):39–56, May 2020. ISSN 2641-8770. doi: 10.1109/JSAIT.2020.2991563. URL <https://ieeexplore.ieee.org/document/9084378>. Conference Name: IEEE Journal on Selected Areas in Information Theory.
- Pajot, A., Bezenac, E. d., and Gallinari, P. Unsupervised Adversarial Image Reconstruction. In *International Conference on Learning Representations*, September 2018.
- Ronneberger, O., Fischer, P., and Brox, T. U-Net: Convolutional Networks for Biomedical Image Segmentation. In Navab, N., Hornegger, J., Wells, W. M., and Frangi, A. F. (eds.), *Medical Image Computing and Computer-Assisted Intervention – MICCAI 2015*, pp. 234–241, 2015. doi: 10.1007/978-3-319-24574-4_28.
- Shen, L., Pauly, J., and Xing, L. NeRP: Implicit Neural Representation Learning With Prior Embedding for Sparsely Sampled Image Reconstruction. *IEEE Transactions on Neural Networks and Learning Systems*, 35(1):770–782, January 2024. ISSN 2162-2388. doi: 10.1109/TNNLS.2022.3177134. URL <https://ieeexplore.ieee.org/document/9788018>. Conference Name: IEEE Transactions on Neural Networks and Learning Systems.
- Tachella, J., Chen, D., and Davies, M. Unsupervised Learning to Solve Inverse Problems: Application to Single-Pixel Imaging. In *XXVIIIème Colloque Francophone de Traitement du Signal et des Images (GRETSI 2022)*, September 2022.
- Tachella, J., Chen, D., Hurault, S., Terris, M., and Wang, A. DeepInverse: A deep learning framework for inverse problems in imaging, June 2023. URL <https://github.com/deepinv/deepinv>.
- Tachella, J., Davies, M., and Jacques, L. UNSURE: self-supervised learning with Unknown Noise level and Stein’s Unbiased Risk Estimate, February 2025. URL <http://arxiv.org/abs/2409.01985>. arXiv:2409.01985 [stat].
- Wang, A. and Davies, M. Fully Unsupervised Dynamic MRI Reconstruction via Diffeo-Temporal Equivariance, October 2024a. URL <http://arxiv.org/abs/2410.08646>. arXiv:2410.08646 [eess].
- Wang, A. and Davies, M. Perspective-Equivariance for Unsupervised Imaging with Camera Geometry, March 2024b. arXiv:2403.09327 [cs, eess].

Yaman, B., Hosseini, S. A. H., Moeller, S., Ellermann, J., Uğurbil, K., and Akçakaya, M. Self-supervised learning of physics-guided reconstruction neural networks without fully sampled reference data. *Magnetic Resonance in Medicine*, 84(6):3172–3191, 2020. doi: 10.1002/mrm.28378.

Zbontar, J., Knoll, F., Sriram, A., Murrell, T., Huang, Z., Muckley, M. J., Defazio, A., Stern, R., Johnson, P., Bruno, M., Parente, M., Geras, K. J., Katsnelson, J., Chandarana, H., Zhang, Z., Drozdal, M., Romero, A., Rabbat, M., Vincent, P., Yakubova, N., Pinkerton, J., Wang, D., Owens, E., Zitnick, C. L., Recht, M. P., Sodickson, D. K., and Lui, Y. W. fastMRI: An Open Dataset and Benchmarks for Accelerated MRI, November 2018. URL <https://arxiv.org/abs/1811.08839v2>.

Zeng, G., Guo, Y., Zhan, J., Wang, Z., Lai, Z., Du, X., Qu, X., and Guo, D. A review on deep learning MRI reconstruction without fully sampled k-space. *BMC Medical Imaging*, 21(1):195, December 2021. ISSN 1471-2342. doi: 10.1186/s12880-021-00727-9. URL <https://doi.org/10.1186/s12880-021-00727-9>.

Supplementary Material

A. Equivalence of Artifact2Artifact and SSDU

Proposition (Unpaired Artifact2Artifact as sum of SSDU losses). Consider the Artifact2Artifact (Liu et al., 2020) scenario where $\mathbf{y}_i^{(k)}$ be independent sets of measurements of the same subject i (e.g. arriving in a stream) such that $\mathbf{y}_i = \bigcup_k \mathbf{y}_i^{(k)} \in \mathbb{R}^m$ is the full undersampled measurement from one acquisition i (i.e. there are no more measurements of the same subject). $\mathbf{A}_i^{(k)\top} \mathbf{y}_i^{(k)}$ are then the independent "artifact"-corrupted images. The Artifact2Artifact loss draws a pair k, l randomly at each iteration and constructs the loss

$$\mathcal{L}_{A2A}^{(k,l)} = \mathcal{L}(\mathbf{A}_i^{(l)} f_{\theta}(\mathbf{y}_i^{(k)}, \mathbf{A}_i^{(k)}), \mathbf{y}_i^{(l)})$$

where $\mathbf{A}_i^{(k)}, \mathbf{A}_i^{(l)}$ are the operators associated with each measurement. We can then write this as the overlapping SSDU loss (Yaman et al., 2020, Fig. 5) by setting $\mathbf{A}_i^{(k)} = \mathbf{M}_k \mathbf{A}_i, \mathbf{A}_i^{(l)} = \mathbf{M}_l \mathbf{A}_i, \mathbf{y}_i^{(k)} = \mathbf{M}_k \mathbf{y}_i, \mathbf{y}_i^{(l)} = \mathbf{M}_l \mathbf{y}_i$ where $\mathbf{M}_k, \mathbf{M}_l$ are two overlapping mask subsampling sets. Then

$$\mathcal{L}_{A2A} = \sum_k \sum_{l \neq k} \mathcal{L}_{SSDU}^{(k,l)}$$

B. Data and hyperparameter details

We use a subset of the FastMRI dataset for our experiments. We take the middle slice of 455 brain volumes, use the provided 320×320 root-sum-square reconstructions as ground truth, normalise them to $[0, 1]$ and simulate measurements using an undersampled Fourier transform. We randomly create train-test datasets with 80-20 split. The knee dataset is created similarly for 973 slices. For the subsampling masks, we use random 1D Gaussian masking with 6x acceleration and 8% autocalibration lines kept in the centre. For the denoiser of our unrolled network, we use a residual U-Net with no batch norm of depth 4, with a total of 8.6M parameters. We train with the Adam optimiser at $1e-3$ learning rate, although we tweak this per method down to $1e-5$ to achieve convergence.

For loss functions involving measurement splitting (i.e. SSDU), we use a 2D Gaussian splitting mask with $\rho = 0.6$ following (Yaman et al., 2020). For losses involving equivariant imaging, we draw randomly a group transform at each iteration; for rotation the group being $G = \text{SO}(\mathbb{R}^2)$ and for diffeomorphisms $G = \text{Diffeo}(\mathbb{R}^2)$

All components of our experiments are implemented using DeepInverse (Tachella et al., 2023). We provide a demo below and full code at [this URL](#).

C. Python code for running experiments using DeepInverse

The following Python code can be used to train a reconstruction algorithm with the methods considered in this paper, where the loss functions `loss` can be replaced by those listed in Table 1.

```
import deepinv as dinv
import torch

# Define forward problem A
physics_generator = dinv.physics.generator.GaussianMaskGenerator((320, 320), acceleration=4)
physics = dinv.physics.MRI((320, 320))

# Define FastMRI dataset x
dataset = dinv.datasets.SimpleFastMRISliceDataset("data", train=True, download=True)
train_dataset, test_dataset = torch.utils.data.random_split(dataset, (0.8, 0.2))

# Simulate measurements (x, y)
dataset_path = dinv.datasets.generate_dataset(
    train_dataset=train_dataset,
    test_dataset=test_dataset,
    physics=physics,
    physics_generator=physics_generator,
    save_physics_generator_params=True,
    save_dir="data"
)

train_dataset = dinv.datasets.HDF5Dataset(dataset_path, split="train", load_physics_generator_params=True)
test_dataset = dinv.datasets.HDF5Dataset(dataset_path, split="test", load_physics_generator_params=True)

train_dataloader = torch.utils.data.DataLoader(train_dataset, shuffle=True)
```

Benchmarking Self-Supervised Methods for Accelerated MRI Reconstruction

Loss	PSNR \uparrow	SSIM \uparrow
MOI	30.29	.8651
EI (rotate)	30.26	.8523
EI (diffeo)	31.26	.8741
MO-EI (rotate)	30.62	.8575
MO-EI (diffeo, ours)	32.14	.8846

Table 5. Ablation of components of our proposed loss function on brain dataset.

Loss	PSNR \uparrow	SSIM \uparrow
Zero-filled	27.98	.7041
MC	27.98	.7040
EI	31.08	.7582
MOI	31.45	.7787
SSDU	10.91	.4131
Noise2Inverse	11.22	.3969
MO-EI (ours)	31.91	.7848
(Supervised)	(32.68)	(.8141)

Table 6. Test set results for 6x accelerated MRI on FastMRI knee dataset. Best unsupervised method in **bold**.

```

test_dataloader = torch.utils.data.DataLoader(test_dataset)

# Define reconstruction  $f_\theta$ 
denoiser = dinv.models.UNet(2, 2, scales=3)
model = dinv.utils.demo.demo_mri_model(denoiser=denoiser, num_iter=3)

# Define loss  $\mathcal{L}$ 
loss = ...

trainer = dinv.Trainer(
    model = model,
    physics = physics,
    optimizer = torch.optim.Adam(model.parameters(), lr=1e-3),
    train_dataloader = train_dataloader,
    eval_dataloader = test_dataloader,
    epochs = 100,
    losses = loss,
    metrics = dinv.metric.PSNR(complex_abs=True),
)

trainer.train()

```

D. Ablation

We ablate for the components of our proposed loss function by interpolating between existing methods MOI and EI and our method MO-EI, and report results in Table 5.

E. Additional results

We report results of experiments comparing methods trained on the knee dataset in Fig. 6 and Table 6.

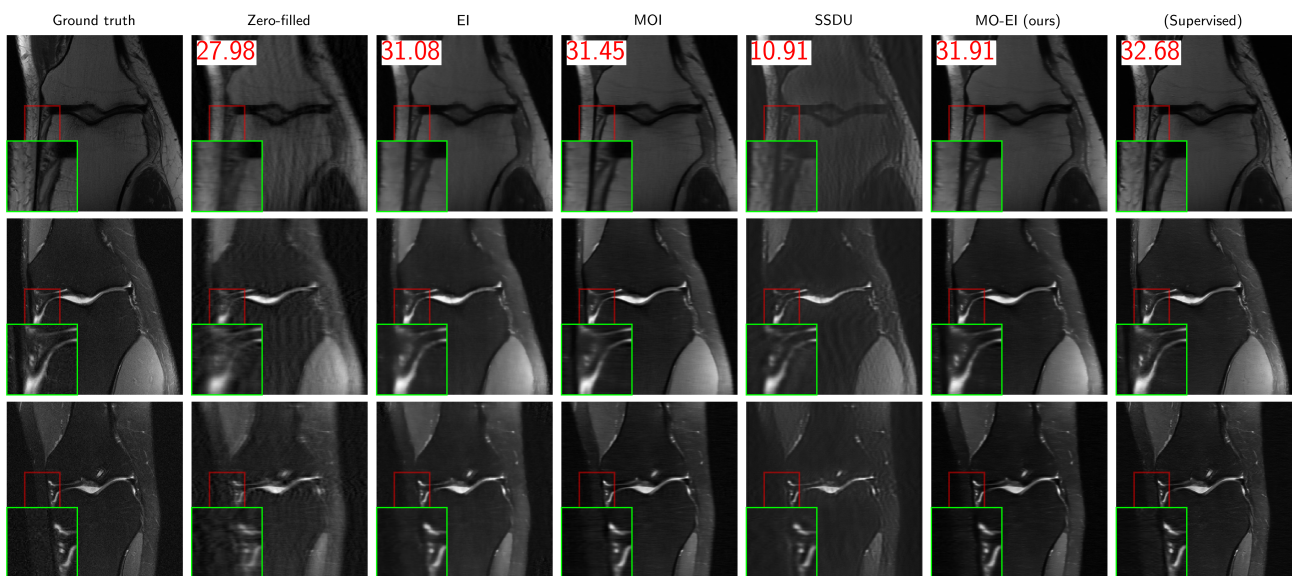


Figure 6. Sample reconstructions for 6x accelerated knee MRI reconstruction with average test-set PSNR labelled.